# Functional Differences in Engineered Myocardium from Embryonic Stem Cell-Derived versus Neonatal Cardiomyocytes

Feinberg, Adam W.; Ripplinger, Crystal M.; van der Meer, Peter; Sheehy, Sean P.; Domian, Ibrahim; Chien, Kenneth R.; Parker, Kevin Kit

*Published in:*
Stem Cell Reports

*DOI:*
10.1016/j.stemcr.2013.10.004



*Publication date:*
2013

Stem Cell Reports
Report
OPEN ACCESS

# Functional Differences in Engineered Myocardium from Embryonic Stem Cell-Derived versus Neonatal Cardiomyocytes

Adam W. Feinberg,[1,3,4,6] Crystal M. Ripplinger,[1,3,4,6] Peter van der Meer,[2,5,6] Sean P. Sheehy,[1,3,4] Ibrahim Domian,[2,3] Kenneth R. Chien,[2,3] and Kevin Kit Parker[1,2,3,4,*]
[1]Disease Biophysics Group, School of Engineering and Applied Sciences, Harvard University, Cambridge, MA 02138, USA
[2]Cardiovascular Research Center, Massachusetts General Hospital, Boston, MA 02114, USA
[3]Harvard Stem Cell Institute, Harvard University, Cambridge, MA 02138, USA
[4]Wyss Institute of Biologically Inspired Engineering, Harvard University, Boston, MA 02115, USA
[5]Department of Cardiology, University Medical Center Groningen, University of Groningen, 9700 RB Groningen, The Netherlands
[6]These authors contributed equally to this work
*Correspondence: kkparker@seas.harvard.edu
http://dx.doi.org/10.1016/j.stemcr.2013.10.004


## SUMMARY

Stem cell-derived cardiomyocytes represent unique tools for cell- and tissue-based regenerative therapies, drug discovery and safety, and studies of fundamental heart-failure mechanisms. However, the degree to which stem cell-derived cardiomyocytes compare to mature cardiomyocytes is often debated. We reasoned that physiological metrics of engineered cardiac tissues offer a means of comparison. We built laminar myocardium engineered from cardiomyocytes that were differentiated from mouse embryonic stem cell-derived cardiac progenitors or harvested directly from neonatal mouse ventricles, and compared their anatomy and physiology in vitro. Tissues assembled from progenitor-derived myocytes and neonate myocytes demonstrated similar cytoskeletal architectures but different gap junction organization and electromechanical properties. Progenitor-derived myocardium had significantly less contractile stress and slower longitudinal conduction velocity than neonate-derived myocardium, indicating that the developmental state of the cardiomyocytes affects the electromechanical function of the resultant engineered tissue. These data suggest a need to establish performance metrics for future stem cell applications.

## INTRODUCTION

Cardiomyocytes can be derived from a variety of sources, including embryonic stem cells (ESCs) (Anderson et al., 2007; Braam et al., 2008; Caspi et al., 2007), induced pluripotent stem cells (iPSCs) (Gai et al., 2009; Zhang et al., 2009), adult stem cells (Beltrami et al., 2003), and direct reprogramming from fibroblasts (Ieda et al., 2010). Significant efforts have been focused on the potential of these cells to repair the heart following myocardial infarction (MI) or to serve as in vitro models of disease. The standard approach for assessing the differentiated state of these derived myocytes has been to determine mRNA, miRNA, and protein expression, as well as the electrophysiological characteristics of myocytes via patch-clamp or calcium imaging (Genead et al., 2010; Sirish et al., 2012). These criteria are important, but they offer an incomplete assessment of the myocyte's physiology.

Cardiac tissue engineering may provide a tool for evaluating stem cell-derived myocytes. In previous studies, primary harvest rodent (Alford et al., 2010; Baar et al., 2005; Feinberg et al., 2007; Zimmermann et al., 2004) and ESC-derived cardiac myocytes (Domian et al., 2009; Guo et al., 2006; Stevens et al., 2009) were used as building substrates for engineered tissues whose function could be rigorously evaluated. These studies demonstrated that engineered tissues can be used as experimental platforms to examine how stem cell-derived cardiac myocytes spontaneously assemble the subcellular, cellular, and supracellular architectures required to facilitate uniform spread of the action potential (AP) and ordered contraction.

We reasoned that we could use engineered tissues as a common test bed for cardiac myocytes from different sources to compare their inherent ability to build themselves and collectively function. Previously, we identified specific subsets of *islet-1*-expressing, ESC-derived cardiac progenitors that are completely committed to the ventricular lineage, and demonstrated that we could differentiate these mouse progenitor cells into cardiac myocytes (progenitor-derived myocytes) and use them to build laminar myocardium (Domian et al., 2009). Here, we built upon that work by conducting a detailed structural and functional analysis of those engineered tissues. As a benchmark for comparison, we engineered similar tissues from neonatal mouse ventricular myocytes. Our results suggest that engineered myocardium from these different sources have distinct functional differences that are critically important for the assessment of such cells for scientific and therapeutic applications.

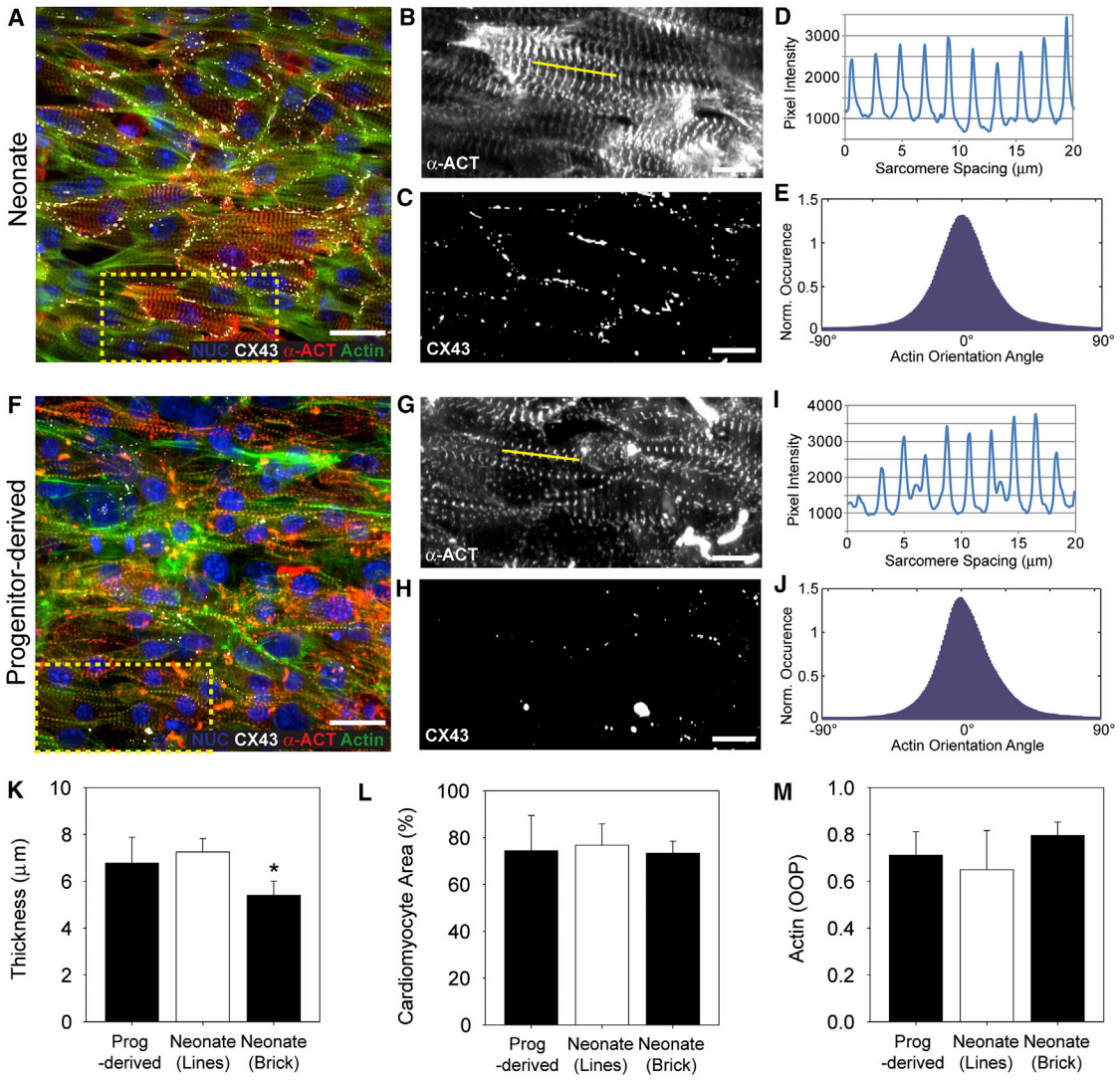


**Figure 1. Structural Analysis of Engineered Myocardium from Neonate Myocytes and Progenitor-Derived Myocytes**

(A) Neonate-derived myocardium had uniaxial cell alignment with sarcomere and Cx43 expression.

(B) At higher magnification (dashed yellow box in A), the sarcomeric α-actinin revealed Z disks with lateral registration spanning across cells.

(C) CX43 was localized to the cell-cell border between adjacent myocytes, suggesting electrical coupling.

(D) Intensity profile of Z-disk staining along a myofibril (yellow line in B) shows normal spacing of 1.99 ± 0.24 μm.

(E) Cytoskeletal orientation (actin filaments) in the neonate myocytes was uniaxially aligned in the direction of the underlying FN-patterned substrate.

(F) Progenitor-derived myocardium also had uniaxial cell alignment with sarcomere and CX43 expression.

(G) At higher magnification (dashed yellow box in F), the sarcomeric α-actinin revealed Z disks with distinct sarcomeres, but decreased lateral registration as compared with neonate myocytes.

(H) CX43 was localized to the cell-cell border between myocytes, but at decreased frequency as compared with neonate myocytes, suggesting decreased electrical coupling.

(I) Intensity profile of Z-disk staining along a myofibril (yellow line in G) shows normal spacing of 2.01 ± 0.19 μm.

(J) Cytoskeletal orientation (actin filaments) in progenitor-derived myocytes was uniaxially aligned in the direction of the underlying FN-patterned substrate.

(K) The thickness of the engineered myocardium was statistically different for the neonate myocytes on the brick pattern versus the neonate myocytes on the line pattern and the progenitor-derived myocytes (ANOVA with Holm-Sidak pairwise comparison, *$p < 0.025$).

(L) The number of myocytes that stained positive for sarcomeric α-actinin was statistically equivalent between the progenitor- and neonate-derived myocardia (ANOVA, $p = 0.871$).

*(legend continued on next page)*

## RESULTS

### Structural Analysis of Engineered Myocardium

We reasoned that we could use soft lithography and muscular thin films (MTFs), as previously described (Alford et al., 2010; Domian et al., 2009; Feinberg et al., 2007, 2012), to build cardiac muscle engineered with progenitor-derived and neonatal cardiac myocytes, and assess its structural, electrophysiological, and contractile properties. We isolated progenitor-derived myocytes from a double-reporter mouse ESC line using fluorescence-activated cell sorting (FACS) (Figure S1 available online), which we previously showed differentiate into >90% ventricular myocytes based on the AP morphology revealed by patch-clamp (Domian et al., 2009). We were able to engineer laminar, anisotropic myocardium by using micropatterned culture surfaces of alternating 20-μm-wide lines of fibronectin (FN) and Pluronics F-127 (Figure S2A; Domian et al., 2009). For neonate myocytes, which failed to form tissues in these conditions, we adopted two alternative approaches. First, we used a softer Sylgard 527 polydimethylsiloxane (PDMS) (Palchesko et al., 2012) to build the same tissue on alternating 20-μm-wide lines of high- and low-density FN (Figure S2B) for electrophysiological experiments. Second, we developed an alternative micropattern of FN rectangles organized in a two-dimensional (2D) pattern similar to a brick wall (Figure S2C), because the neonate tissues folded the softer MTFs. With this brick wall micropattern, we were able to engineer 2D myocardium of neonate myocytes on Sylgard 184 and perform MTF experiments to measure contractility.

We quantified the structure of the engineered myocardium using immunofluorescence staining of myofibrils and gap junctions in the myocytes. Both the progenitor- and neonate-derived tissues contained large numbers of myofibrils oriented uniaxially, and the myocytes coupled via Cx43 gap junctions (Figures 1A and 1F). Neonate-derived myocardium had well-developed myofibrils with lateral registration of Z disks between myofibrils both within myocytes and across transverse cell-cell borders (Figure 1B). The progenitor-derived myocardium had a similar network of myofibrils (Figure 1G), but the staining pattern of the sarcomeric α-actinin suggested an immature myofibrillar architecture. The neonate-derived myocardium had robust Cx43 staining at the cell-cell junctions at the myocyte periphery (Figure 1C), consistent with the Cx43 peripheral localization reported for engineered myocardium from neonate myocytes (Beauchamp et al., 2006; Thomas et al., 2000) and cultured neonatal rat ventricular myocytes (Feinberg et al., 2007). The progenitor-derived myocardium also exhibited Cx43 at the cell-cell junctions at the myocyte periphery (Figure 1H); however, there were fewer visible Cx43 plaques, suggesting a difference in cell-cell electrical coupling as compared with neonate-derived tissues.

We quantified the myofibrillar organization of the progenitor- and neonate-derived myocardium to test whether the different tissue types could be engineered with similar structural properties. Intensity plots (Figures 1D and 1I) of the sarcomeric α-actinin staining along myofibrils (yellow line in Figures 1B and 1G) enabled quantification of the average Z-disk spacing across tissue types. The contractile force generated by the sarcomere is length dependent (de Tombe et al., 2010), but there was no difference between the Z-disk spacing along the myofibrils, which was 2.01 ± 0.19 μm and 1.99 ± 0.24 μm for progenitor- and neonate-derived myocardium, respectively (t test, $p = 0.227$). We quantified myofibril organization by determining F-actin orientation at each pixel within the image to create a histogram of orientation angles (Figures 1E and 1J; Bray et al., 2010; Pong et al., 2011). These data were used to determine the orientational order parameter (OOP) of each tissue type as a global metric of myofibril alignment. We structurally analyzed the progenitor-derived myocardium and both types of neonate myocardium (the line and brick-wall micropatterns). The progenitor- and neonate-derived myocardium all had statistically equivalent actin alignment (Figure 1M; $n = 6$ per tissue type). We also quantified the volume of muscle in the engineered tissues by staining the sarcomeric α-actinin in the Z disks to visualize only the myocytes. The tissue thickness in the z axis perpendicular to the coverslip ranged from 5 to 7 μm (Figure 1K). Although the neonate brick-wall myocardium was thinner by ~1 μm, all tissues were still only one cell layer thick and did not multilayer. Approximately 75% of cells in each tissue stained positive for sarcomeric α-actinin, with no statistical difference between tissue types (Figure 1L). These data suggest that tissues engineered from progenitor-derived and neonatal ventricular myocytes have a comparable ability to generate aligned myofibrils, but a different capacity to generate Cx43 gap junctions.

### Electrophysiology of Engineered Myocardium

To analyze the electrophysiological properties of the myocardium, we conducted optical mapping experiments

(M) Cytoskeletal organization as quantified by actin alignment (example histograms shown in E and J) was analyzed using the OOP, and demonstrated that the progenitor-derived and two types of neonate-derived myocardia were statistically equivalent (Kruskal-Wallis ANOVA on ranks, $p = 0.194$).

Scale bars, 25 μm (A and F) and 10 μm (B, C, G, and H). Sample sizes for (K), (L), and (M): progenitor-derived ($n = 6$), neonate lines ($n = 5$), and neonate brick ($n = 6$). Error bars indicate SD.

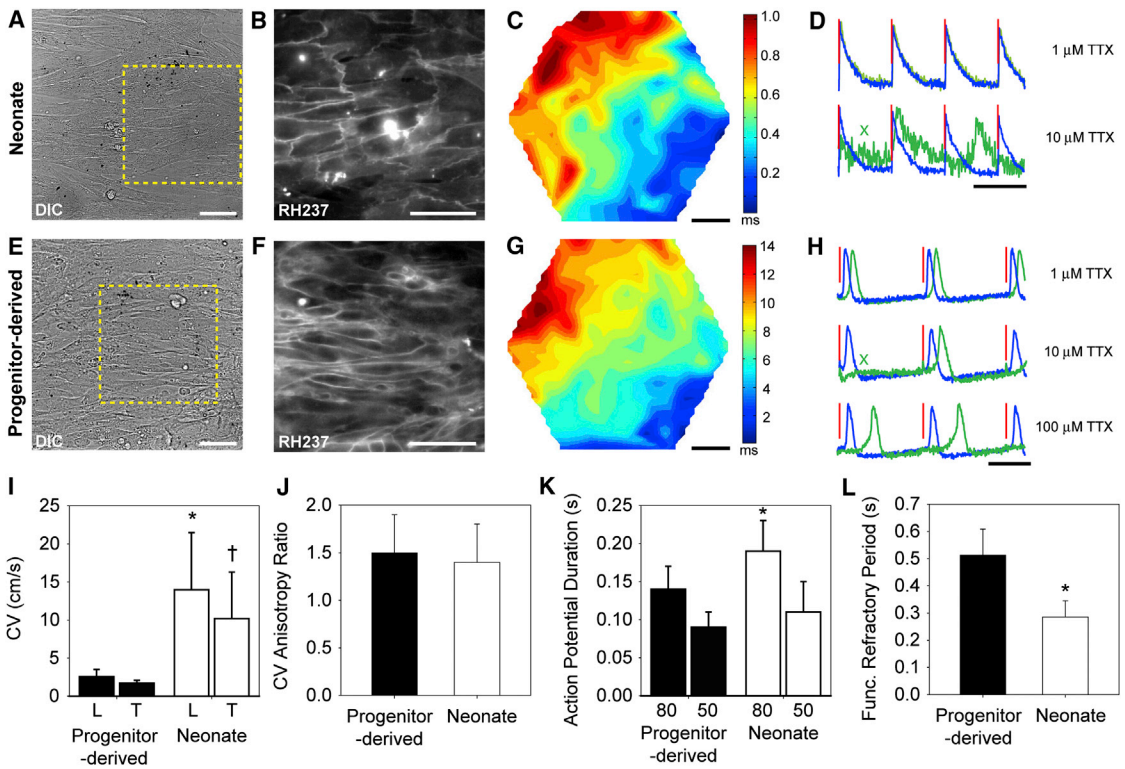


**Figure 2. Electrophysiology of Engineered Myocardium from Neonate Myocytes and Progenitor-Derived Myocytes Shows the Formation of a Functional Syncytium**

(A) Differential interference contrast (DIC) image of engineered neonatal mouse myocardium.

(B) Image of the region highlighted by the dashed yellow box in (A) showing cell-cell borders with the voltage-sensitive fluorescent dye RH-237.

(C) Example activation map of AP propagation.

(D) Example AP traces (blue, no treatment; green, TTX treatment; red, pacing stimuli) showing conduction block at 10 μM TTX (green X).

(E) Bright-field DIC image of progenitor-derived myocardium.

(F) Image of the region highlighted by the dashed yellow box in (E) showing cell-cell borders with the voltage-sensitive fluorescent dye RH-237.

(G) Example activation map of AP propagation. Note the later activation times compared with (C).

(H) Example AP traces (blue, no treatment; green, TTX treatment; red, pacing stimuli) show that conduction block does not occur even at 100 μM TTX, although conduction delay is observed. Also note the slow diastolic depolarization compared with the neonate mouse tissue in (D).

(I) Longitudinal (L) and transverse (T) CVs are substantially decreased in progenitor-derived myocardium compared with neonate-derived myocardium (*$p < 0.001$ and $^{\dagger}p = 0.003$ for neonate- versus progenitor-derived).

(J) The anisotropy ratio is equivalent between the engineered tissues ($p = 0.380$).

(K) APD at 50% and 80% repolarization. The progenitor-derived myocardium has a significantly shorter $APD_{80}$ than the neonate-derived myocardium (*$p = 0.020$).

(L) The FRP is significantly shorter in the neonate-derived myocardium than in the progenitor-derived myocardium, indicating post-repolarization refractoriness and/or slow conduction (*$p = 0.004$).

Scale bars are 50 μm (A–C and E–G) and 500 ms (D and H). Statistical significance is based on Holm-Sidak multiple pairwise comparisons in (I) and (K), and Student's t test in (J) and (L). Sample sizes in (I) and (J): progenitor-derived ($n = 7$) and neonate ($n = 8$); (K): progenitor-derived ($n = 8$) and neonate ($n = 8$); and (L): progenitor-derived ($n = 5$) and neonate ($n = 6$). Error bars indicate SD.

using voltage-sensitive membrane dyes and Blebbistatin as an excitation-contraction uncoupler. The neonate- and progenitor-derived myocardia formed continuous monolayers (Figures 2A and 2E, respectively), as indicated by RH237 staining (Figures 2B and 2F). Bipolar pacing stimuli resulted in activation wavefront propagation in both tissue types (Figures 2C and 2G). Progenitor-derived myocardium had considerably slower wavefront propagation, as indicated by later activation times (Figures 2G versus 2C), and significantly decreased longitudinal and transverse

conduction velocities (CVs; Figure 2I). The neonate longitudinal CVs were lower than those previously reported for patterned neonate strands (Thomas et al., 2000), but studies in neonatal rat ventricular myocytes have shown that CVs are higher in myocardial strands than in tissues (Feinberg et al., 2012). Despite these differences in CV, the ratio of longitudinal-to-transverse CV (referred to as the anisotropy ratio) was the same for neonate- and progenitor-derived myocardia (Figure 2J). This suggests a similar degree of myocyte alignment between tissue types, in agreement with the actin alignment data (Figure 1M) and previously reported anisotropy ratios for engineered myocardium assembled from neonate rat ventricular myocytes (Bursac et al., 2002; Feinberg et al., 2012) and mouse heart (Gutstein et al., 2001). The AP morphology varied (Figure 2D and 2H), with the progenitor-derived myocardium exhibiting slow diastolic depolarization between APs and a shorter mean AP duration (APD) at both 50% and 80% repolarization (Figure 2K). However, despite the shorter APD, the progenitor-derived myocardium had a longer functional refractory period (FRP) than the neonate-derived myocardium (Figure 2L).

The tissues responded differently to the Na-channel blocker tetrodotoxin (TTX). Increasing concentrations of TTX resulted in slowing of conduction in the progenitor-derived myocardium, as evidenced by longer conduction delays from the pacing stimulus to local activation (Figure 2H, blue untreated versus green TTX-treated APs). Occasional conduction block was observed (green "X" in Figure 2H, middle panel). However, APs continued to propagate even at the highest concentration of TTX (100 μM) in all three samples in which TTX was administered. In contrast, one neonate-derived tissue exhibited complete conduction block at 1 μM TTX and all samples exhibited complete or near-complete block (similar to Figure 2D) at 10 μM TTX. This result suggests that the progenitor-derived myocytes can generate APs without a significant contribution from Na channels.

### Contractility of Engineered Myocardium

We assessed contractility using the MTF assay to quantify peak systolic stress generated under various pacing conditions. Note that the MTF contractility assay approximates a single lamellar layer of the ventricular wall and is effectively an isometric measurement in which the radius of curvature changes as a function of diastolic and systolic stress (Alford et al., 2010; Feinberg et al., 2007). The PDMS film thickness was calibrated such that the neonate- and progenitor-derived MTFs produced comparable deformations at peak systole (Figures 3A and 3D). Neonate-derived myocardium had a spontaneous contractile frequency of $\geq$1 Hz, with individual MTFs being captured at pacing frequencies between 1 and 10 Hz (Figure 3B). All of the neonate mouse MTFs responded to pacing at 3 and/or 4 Hz, corresponding to the resting heart rate of neonatal mice (Hou and Burggren, 1989). In comparison, progenitor-derived myocardium had a spontaneous contractile frequency, typically <1 Hz, with individual MTFs captured between 0.5 and 5 Hz (Figure 3E). All of the progenitor-derived MTFs responded to pacing at 1 and 2 Hz, corresponding to the embryonic mouse heart rate at 10–11 days of gestation (Gui et al., 1996). Specifically, the maximum frequency at which most progenitor- and neonate-derived MTFs could be paced (2 Hz and 4 Hz, respectively; Figures 3B and 3E) was the same as the FRP. These results suggest differences in the spontaneous activity of the myocardial tissues, the excitability of the tissues, and the maximum contraction rates as a function of myocyte maturity.

The neonate-derived myocardium generated significantly greater peak systolic stresses than the progenitor-derived myocardium. Example contraction plots for neonate-derived myocardium (Figure 3C) show that stress varied with pacing frequency, but was on the order of 5–10 kPa over a pacing range of 2–8 Hz. Although neonatal mouse myocardium has been shown to have a positive force-frequency relationship (Xi et al., 2010), our tissues derived from neonate myocytes had a negative force-frequency relationship observed from 3–8 Hz pacing (Figure 3C), consistent with other reports for mouse and rat engineered heart tissue (de Lange et al., 2011; Feinberg et al., 2012). In contrast, contraction of the progenitor-derived tissues (Figure 3F) showed that peak stress was substantially lower at ~1 kPa over a range of 1–3 Hz. The flat force-frequency relationship for the progenitor-derived myocardium over the 1–3 Hz pacing range does not resemble neonatal mouse myocardium or neonate-derived myocardium, but is consistent with other reports for mouse ESC-derived engineered myocardium (Xi et al., 2010). A comparison of the peak systolic stress between tissue types at multiple pacing frequencies illustrates this difference in contractility (Figure 3G). Peak systolic stress varied significantly between the neonate- and progenitor-derived tissues at all pacing frequencies ($p < 0.001$), but there was no difference within each tissue type (two-way ANOVA and the Holm-Sidak method for multiple pairwise comparisons).

## DISCUSSION

The current study was motivated by a simple question: how comparable are our progenitor-derived myocytes to neonatal myocytes? The differentiation of stem cells into cardiac myocytes is typically assessed in a manner that provides little insight into how they function as a tissue, and

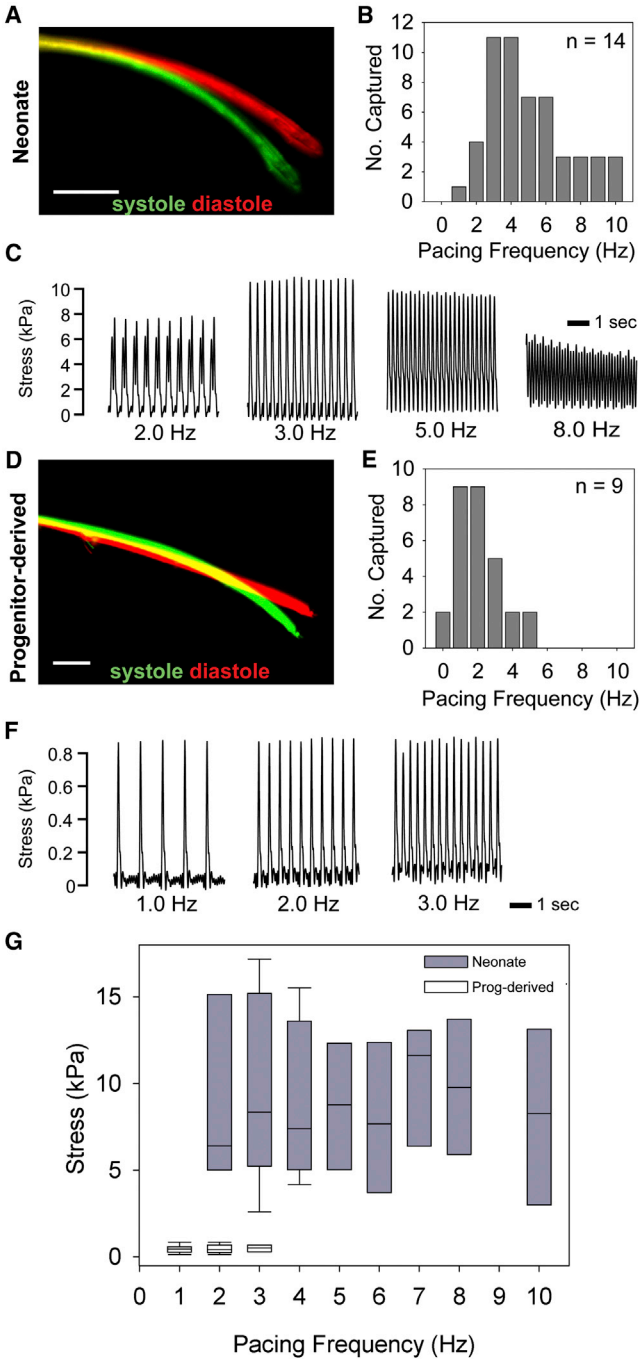


**Figure 3. Contractility of Neonate- and Progenitor-Derived Engineered Myocardia**

(A) Representative neonate-derived MTF in diastole (red) and peak systole (green). Scale bars are 500 μm.

(B) Histogram of the number of neonate-derived MTFs captured as a function of stimulation frequency.

(C) Example plots of contractile stress generated at various pacing frequencies in a neonate-derived MTF.

(D) Representative progenitor-derived MTF in diastole (red) and peak systole (green). Scale bars are 500 μm.

(E) Histogram of the number of progenitor-derived MTFs captured as a function of stimulation frequency.

(F) Example plots of contractile stress generated at various pacing frequencies in a progenitor-derived MTF.

(G) Peak systolic stress as a function of stimulation frequency. The box plots range from the 25th to 75th percentile, with the median indicated by the solid line, and whiskers indicate the 10th and 90th percentiles for pacing frequencies where $n \geq 9$ MTFs responded. There is a statistically significant difference between the neonate- and progenitor-derived myocardia (two-way ANOVA, $p < 0.01$). The sample sizes for each tissue type and pacing frequency are indicated graphically in (B) and (E).

instead relies on the expression of lineage markers to infer functionality (Sartiani et al., 2007). Thus, we chose a set of metrics that define the most important functional characteristic of cardiac myocytes: the ability to self-organize into and function as laminar myocardium.

Mature ventricular myocytes rebuild their contractile cytoskeleton and cell-cell junctions continuously. We assessed the functional implications of the subcellular, cellular, and multicellular architectures within the engineered tissues to determine whether the electrophysiological and contractile performance of stem cell-derived myocytes was comparable to that of myocytes isolated directly from the ventricular myocardium. To perform this comparison, we evaluated the cellular alignment, gap junction localization, and cytoskeletal architecture in engineered tissues. Physiological comparisons of the two tissues were based on techniques described in previous studies of engineered tissues (Bursac et al., 2002; Chung et al., 2011; Feinberg et al., 2012) and classical physiology. Our findings suggest that immature cardiac myocytes of stem cell origin may have significant deficits in tissue genesis as compared with neonates.

As expected, these structural inadequacies were reflected functionally, in that progenitor-derived tissues had significantly impaired contractility and electrophysiology with respect to neonate-derived tissues. These differences could not be predicted from single-cell measurements, as cell-cell coupling, gap junction formation, and lateral registration of myofibrils across cells are emergent properties of myocardial tissues. The contractility of 3D tissues engineered with human ESC- and iPSC-derived myocytes varies widely, with peak systolic stresses in the range of 0.1–10 kPa reported in previous studies (Kensah et al., 2013; Tulloch et al., 2011; Zhang et al., 2013). These studies demonstrated the ability to engineer human myocardium, but also illustrated the difficulty of comparing experiments employing different cell sources, culture conditions, scaffolds, and analysis methods. In comparison, the MTF contractility assay is simple to implement, is reproducible, and has been demonstrated to work with a wide range of cell types,

including progenitor-derived myocytes (Domian et al., 2009), neonatal rat ventricular myocytes (Feinberg et al., 2007, 2012), skeletal muscle (Sun et al., 2013), and vascular smooth muscle (Alford et al., 2010). Thus, the MTF system serves as a platform for engineering myocardium with the same tissue alignment but from different cell sources, enabling comparable evaluations of the myogenic and functional potential of these cells in a reproducible system.

Although we made a significant effort to ensure that the progenitor- and neonate-derived myocardia were as structurally similar as possible, it should be noted that there are limitations inherent to using these different cell sources. Specifically, we cannot completely control the heterogeneity of the cell population. For both tissue types, the area of the MTF covered by cardiomyocytes was statistically equivalent (Figure 1L); however, the ~25% remaining cells were not identified. For neonate-derived myocardium, the noncardiomyocytes in the primary harvest cells will be a combination of cardiac fibroblasts, endothelial cells, and smooth muscle cells. For progenitor-derived myocardium, the noncardiomyocytes in the FACS population will be a combination cardiac progenitors that have differentiated into endothelial cells or smooth muscle cells, or only partially differentiated into one of these cell types or a cardiomyocyte (Chien et al., 2008; Domian et al., 2009). Further, false-positives occur with FACS, so a small percentage of these cells may have differentiated into other cell types. Although we know that noncardiomyocytes cannot contract on the 1 Hz timescale we measure with the MTFs because they lack well-formed sarcomeres, we cannot completely rule out cell-cell coupling or paracrine effects that might impact the electromechanical function of the engineered myocardium. Future studies will need to investigate whether additional FACS, perhaps using a myosin heavy chain reporter, could further purify the cardiomyocyte population and improve the function of the progenitor-derived myocardium.

Clinically, the laminar ventricular myocardium on the MTF is similar to the idealized tissue architecture for a ventricular patch for repair of an MI. Researchers have successfully used human iPSCs (Nelson et al., 2009) and ESCs (Kehat et al., 2004) in rodent MI disease models and autologous mesenchymal stem cells (Katritsis et al., 2005) in human MI patients, and often have been able to improve the ejection fraction (contraction). However, these gains are typically small, often transient, and typically attributed to paracrine effects that induce angiogenesis rather than to cell integration with the host myocardium (Passier et al., 2008). Cell-source selection and the efficacy of the patch may be improved by an in vitro testing platform that is easily translated to clinical application. The MTF platform we used in this study is amenable to thorough in vitro testing, mechanical conditioning, and (potentially) clinical applications involving a broad range of therapeutic parameters (Barron et al., 2003; Radisic et al., 2007).

In conclusion, the observed differences in structure and function between progenitor-derived myocytes and neonate myocytes clearly demonstrate the need to establish metrics for the use of stem cells. A promising method for performing such quality validation studies is to utilize traditional histological and physiological assays to evaluate engineered tissues fabricated from stem cell-derived myocytes. This is important, because as the field moves rapidly toward applications of stem cells in drug discovery, safety pharmacology, in vitro disease modeling, and regenerative medicine, it will be critical for stem cell-derived myocytes to recapitulate the required performance characteristics.

## EXPERIMENTAL PROCEDURES

### Cardiomyocytes from Mouse ESC Lines and Neonatal Ventricles

All procedures were approved by the Harvard University Animal Care and Use Committee. The ESC-derived cardiac progenitor cells (CPCs) were generated and isolated using previously described methods (Domian et al., 2009). Briefly, ESC lines were created from transgenic mice with a combined enhanced GFP (eGFP) and discosoma species Red (dsRed) reporter system to isolate CPCs by FACS. The R+G+ CPCs used in these experiments were previously shown to be highly myogenic and differentiate into myocytes with a ventricular phenotype (process illustrated in Figure S1). CPCs were cultured on coverslips with micropatterned FN lines for 3–5 days to differentiate the cells into cardiac myocytes. They were then trypsinized, resuspended, and seeded onto micropatterned coverslips for 2 days prior to immunohistochemistry and electrophysiological assays, or on MTFs for contractility assays. Neonate myocytes were isolated from 2-day-old neonatal C57/Bl6 mice via a procedure adapted from previously published methods for isolating neonatal rat ventricular myocytes (Alford et al., 2010; Feinberg et al., 2007). Ventricles were extracted, enzymatically dissociated, and resuspended in culture. Myocytes were cultured for 4 days on micropatterned coverslips prior to immunohistochemistry and electrophysiological assays, or on MTFs for contractility assays.

### Engineered Myocardium

The method for engineering the myocardium was adapted from previously published methods (Alford et al., 2010; Domian et al., 2009; Feinberg et al., 2007) and optimized for each cell type and analysis. For progenitor-derived myocytes, coverslips were spin-coated with Sylgard 184 PDMS (Dow Corning). For neonate myocytes, coverslips were spin-coated with either Sylgard 184 PDMS or Sylgard 527 PDMS. The PDMS-coated coverslips were microcontact printed (μCP) with FN using one of three patterns (anisotropic, lines, or bricks; Figure S2). The anisotropic and line patterns consisted of 20-μm-wide, 20-μm-spaced FN lines and backfilled with 1% Pluronics F-127 for progenitor-derived myocytes (Figure S2A) or low-density FN for neonate myocytes on Sylgard 527

(Figure S2B). The brick patten consisted of 20-μm-wide, 100-μm-long FN rectangles spaced 3 μm apart and backfilled with 1% Pluronics F-127 (Figure S2C). The MTFs were fabricated according to published methods using Sylgard 184 (Feinberg et al., 2007) and then patterned with FN lines for the progenitor-derived myocytes or FN bricks for the neonate myocytes.

### MTF Contractility Assay

MTF contractility assays were performed and analyzed according to previously published methods (Alford et al., 2010). Contractility assays were conducted using a custom-built organ bath system with a Petri dish mounted in an aluminum stage plate with integrated resistive heaters that maintained the Tyrode's solution at 36°C ± 1°C. MTF contractions were initiated using parallel platinum wire electrodes to apply field stimulation (Myopacer; IonOptix) consisting of 7–14 V, 10-ms-duration square wave at pacing rates of 1–10 Hz.

### Optical Mapping Experiments

Optical recordings of the transmembrane potential ($V_m$) in the engineered myocardium were performed on days concurrent with the contractility assays. Measurements were carried out in normal Tyrode's solution at 35°C using the voltage-sensitive dye RH237 (Invitrogen) and the excitation-contraction uncoupler Blebbistatin (Calbiochem). To block sodium ion channels, TTX (Sigma) was added at working concentrations of 1, 10, and 100 μM. Fluorescence recordings were obtained using an inverted microscope (Zeiss Axiovert 200) with a 40× objective (Zeiss EC Plan-Neofluar, numerical aperture 1.3). Pacing was applied via bipolar point stimulation from the tips of two platinum wires located ~1 mm above the monolayer. Pacing frequency was increased in steps of 0.5 Hz, and the highest frequency maintained was deemed the FRP. CV vector fields were calculated from interpolated activation maps (Bayly et al., 1998). The APD was calculated at 50% and 80% repolarization from digitized voltage signals low-pass filtered to improve the signal-to-noise ratio.

### Quantitative Immunofluorescence of Cytoskeletal Structure

The engineered myocardium on the PDMS-coated coverslips was fixed and stained at time points concurrent with MTF and optical mapping using a modification of previously published methods (Alford et al., 2010; Feinberg et al., 2007). The Z disks in the sarcomeres were stained with mouse anti-(sarcomeric α-actinin) primary antibody (Sigma) and gap junctions were stained with rabbit anti-Cx43 primary antibody (Sigma). Samples were then concurrently stained with Alexa Fluor 488 goat anti-rabbit and Alexa Fluor 546 goat anti-mouse secondary antibodies, Alexa Fluor 633 phalloidin and 4′,6-diamidino-2-phenylindol (Invitrogen), mounted on microscope slides and imaged with a Zeiss LSM 5 Live laser scanning confocal microscope. Sarcomere spacing along myofibrils was determined from the sarcomeric α-actinin staining using ImageJ (NIH). The thickness and percent area of the engineered myocardium were determined from z stacks of α-actinin using ImageJ to create binary images and custom MATLAB code for quantification. Actin alignment was quantified based on published methods (Bray et al., 2010) and reported as the 2D orientation order parameter (OOP) (Hamley, 2007).

### Statistical Analysis

Statistical analysis for two groups that passed the normality test was conducted using Student's t test, or otherwise with the Mann-Whitney rank sum test. Statistical analysis of more than two groups was conducted using one- or two-way ANOVA followed by multiple pairwise comparison using the Holm-Sidak method. All data were plotted and statistically analyzed using SigmaPlot (Systat Software), with significant difference based on $p < 0.05$.

## SUPPLEMENTAL INFORMATION

Supplemental Information includes Supplemental Experimental Procedures, two figures, and two movies and can be found with this article online at http://dx.doi.org/10.1016/j.stemcr.2013.10.004.

## ACKNOWLEDGMENTS

We thank the Harvard Center for Nanoscale Systems (CNS) for use of their soft-lithography facilities. This work was supported by grant U01 HL100408-02 from the Progenitor Cell Biology Consortium and the National Heart Lung and Blood Institute, National Institutes of Health. P.v.d.M. received financial support from the Netherlands Organization for Scientific Research (VENI grant 016106013).

Received: April 14, 2013
Revised: October 4, 2013
Accepted: October 7, 2013
Published: November 7, 2013

## REFERENCES

Alford, P.W., Feinberg, A.W., Sheehy, S.P., and Parker, K.K. (2010). Biohybrid thin films for measuring contractility in engineered cardiovascular muscle. Biomaterials *31*, 3613–3621.

Anderson, D., Self, T., Mellor, I.R., Goh, G., Hill, S.J., and Denning, C. (2007). Transgenic enrichment of cardiomyocytes from human embryonic stem cells. Mol. Ther. *15*, 2027–2036.

Baar, K., Birla, R., Boluyt, M.O., Borschel, G.H., Arruda, E.M., and Dennis, R.G. (2005). Self-organization of rat cardiac cells into contractile 3-D cardiac tissue. FASEB J. *19*, 275–277.

Barron, V., Lyons, E., Stenson-Cox, C., McHugh, P.E., and Pandit, A. (2003). Bioreactors for cardiovascular cell and tissue growth: a review. Ann. Biomed. Eng. *31*, 1017–1030.

Bayly, P.V., KenKnight, B.H., Rogers, J.M., Hillsley, R.E., Ideker, R.E., and Smith, W.M. (1998). Estimation of conduction velocity vector fields from epicardial mapping data. IEEE Trans. Biomed. Eng. *45*, 563–571.

Beauchamp, P., Yamada, K.A., Baertschi, A.J., Green, K., Kanter, E.M., Saffitz, J.E., and Kléber, A.G. (2006). Relative contributions of connexins 40 and 43 to atrial impulse propagation in synthetic strands of neonatal and fetal murine cardiomyocytes. Circ. Res. *99*, 1216–1224.

Beltrami, A.P., Barlucchi, L., Torella, D., Baker, M., Limana, F., Chimenti, S., Kasahara, H., Rota, M., Musso, E., Urbanek, K., et al. (2003). Adult cardiac stem cells are multipotent and support myocardial regeneration. Cell *114*, 763–776.

Braam, S.R., Denning, C., van den Brink, S., Kats, P., Hochstenbach, R., Passier, R., and Mummery, C.L. (2008). Improved genetic manipulation of human embryonic stem cells. Nat. Methods *5*, 389–392.

Bray, M.-A.P., Adams, W.J., Geisse, N.A., Feinberg, A.W., Sheehy, S.P., and Parker, K.K. (2010). Nuclear morphology and deformation in engineered cardiac myocytes and tissues. Biomaterials *31*, 5143–5150.

Bursac, N., Parker, K.K., Iravanian, S., and Tung, L. (2002). Cardiomyocyte cultures with controlled macroscopic anisotropy: a model for functional electrophysiological studies of cardiac muscle. Circ. Res. *91*, e45–e54.

Caspi, O., Lesman, A., Basevitch, Y., Gepstein, A., Arbel, G., Habib, I.H.M., Gepstein, L., and Levenberg, S. (2007). Tissue engineering of vascularized cardiac muscle from human embryonic stem cells. Circ. Res. *100*, 263–272.

Chien, K.R., Domian, I.J., and Parker, K.K. (2008). Cardiogenesis and the complex biology of regenerative cardiovascular medicine. Science *322*, 1494–1497.

Chung, C.Y., Bien, H., Sobie, E.A., Dasari, V., McKinnon, D., Rosati, B., and Entcheva, E. (2011). Hypertrophic phenotype in cardiac cell assemblies solely by structural cues and ensuing self-organization. FASEB J. *25*, 851–862.

de Lange, W.J., Hegge, L.F., Grimes, A.C., Tong, C.W., Brost, T.M., Moss, R.L., and Ralphe, J.C. (2011). Neonatal mouse-derived engineered cardiac tissue: a novel model system for studying genetic heart disease. Circ. Res. *109*, 8–19.

de Tombe, P.P., Mateja, R.D., Tachampa, K., Ait Mou, Y., Farman, G.P., and Irving, T.C. (2010). Myofilament length dependent activation. J. Mol. Cell. Cardiol. *48*, 851–858.

Domian, I.J., Chiravuri, M., van der Meer, P., Feinberg, A.W., Shi, X., Shao, Y., Wu, S.M., Parker, K.K., and Chien, K.R. (2009). Generation of functional ventricular heart muscle from mouse ventricular progenitor cells. Science *326*, 426–429.

Feinberg, A.W., Feigel, A., Shevkoplyas, S.S., Sheehy, S., Whitesides, G.M., and Parker, K.K. (2007). Muscular thin films for building actuators and powering devices. Science *317*, 1366–1370.

Feinberg, A.W., Alford, P.W., Jin, H., Ripplinger, C.M., Werdich, A.A., Sheehy, S.P., Grosberg, A., and Parker, K.K. (2012). Controlling the contractile strength of engineered cardiac muscle by hierarchal tissue architecture. Biomaterials *33*, 5732–5741.

Gai, H., Leung, E.L.H., Costantino, P.D., Aguila, J.R., Nguyen, D.M., Fink, L.M., Ward, D.C., and Ma, Y.P. (2009). Generation and characterization of functional cardiomyocytes using induced pluripotent stem cells derived from human fibroblasts. Cell Biol. Int. *33*, 1184–1193.

Genead, R., Danielsson, C., Wärdell, E., Kjaeldgaard, A., Westgren, M., Sundström, E., Franco-Cereceda, A., Sylvén, C., and Grinnemo, K.-H. (2010). Early first trimester human embryonic cardiac Islet-1 progenitor cells and cardiomyocytes: immunohistochemical and electrophysiological characterization. Stem Cell Res. (Amst.) *4*, 69–76.

Gui, Y.-H., Linask, K.K., Khowsathit, P., and Huhta, J.C. (1996). Doppler echocardiography of normal and abnormal embryonic mouse heart. Pediatr. Res. *40*, 633–642.

Guo, X.-M., Zhao, Y.-S., Chang, H.-X., Wang, C.-Y., E, L.-L., Zhang, X.A., Duan, C.M., Dong, L.Z., Jiang, H., Li, J., et al. (2006). Creation of engineered cardiac tissue in vitro from mouse embryonic stem cells. Circulation *113*, 2229–2237.

Gutstein, D.E., Morley, G.E., Tamaddon, H., Vaidya, D., Schneider, M.D., Chen, J., Chien, K.R., Stuhlmann, H., and Fishman, G.I. (2001). Conduction slowing and sudden arrhythmic death in mice with cardiac-restricted inactivation of connexin43. Circ. Res. *88*, 333–339.

Hamley, I.W. (2007). Introduction to Soft Matter: Synthetic and Biological Self-Assembling Materials (Chichester, UK: John Wiley & Sons).

Hou, P.-C.L., and Burggren, W.W. (1989). Interaction of allometry and development in the mouse Mus musculus: heart rate and hematology. Respir. Physiol. *78*, 265–280.

Ieda, M., Fu, J.-D., Delgado-Olguin, P., Vedantham, V., Hayashi, Y., Bruneau, B.G., and Srivastava, D. (2010). Direct reprogramming of fibroblasts into functional cardiomyocytes by defined factors. Cell *142*, 375–386.

Katritsis, D.G., Sotiropoulou, P.A., Karvouni, E., Karabinos, I., Korovesis, S., Perez, S.A., Voridis, E.M., and Papamichail, M. (2005). Transcoronary transplantation of autologous mesenchymal stem cells and endothelial progenitors into infarcted human myocardium. Catheter. Cardiovasc. Interv. *65*, 321–329.

Kehat, I., Khimovich, L., Caspi, O., Gepstein, A., Shofti, R., Arbel, G., Huber, I., Satin, J., Itskovitz-Eldor, J., and Gepstein, L. (2004). Electromechanical integration of cardiomyocytes derived from human embryonic stem cells. Nat. Biotechnol. *22*, 1282–1289.

Kensah, G., Roa Lara, A., Dahlmann, J., Zweigerdt, R., Schwanke, K., Hegermann, J., Skvorc, D., Gawol, A., Azizian, A., Wagner, S., et al. (2013). Murine and human pluripotent stem cell-derived cardiac bodies form contractile myocardial tissue in vitro. Eur. Heart J. *34*, 1134–1146.

Nelson, T.J., Martinez-Fernandez, A., Yamada, S., Perez-Terzic, C., Ikeda, Y., and Terzic, A. (2009). Repair of acute myocardial infarction by human stemness factors induced pluripotent stem cells. Circulation *120*, 408–416.

Palchesko, R.N., Zhang, L., Sun, Y., and Feinberg, A.W. (2012). Development of polydimethylsiloxane substrates with tunable elastic modulus to study cell mechanobiology in muscle and nerve. PLoS ONE *7*, e51499.

Passier, R., van Laake, L.W., and Mummery, C.L. (2008). Stem-cell-based therapy and lessons from the heart. Nature *453*, 322–329.

Pong, T., Adams, W.J., Bray, M.-A., Feinberg, A.W., Sheehy, S.P., Werdich, A.A., and Parker, K.K. (2011). Hierarchical architecture influences calcium dynamics in engineered cardiac muscle. Exp. Biol. Med. (Maywood) *236*, 366–373.

Radisic, M., Park, H., Gerecht, S., Cannizzaro, C., Langer, R., and Vunjak-Novakovic, G. (2007). Biomimetic approach to cardiac

tissue engineering. Philos. Trans. R. Soc. Lond. B Biol. Sci. *362*, 1357–1368.

Sartiani, L., Bettiol, E., Stillitano, F., Mugelli, A., Cerbai, E., and Jaconi, M.E. (2007). Developmental changes in cardiomyocytes differentiated from human embryonic stem cells: a molecular and electrophysiological approach. Stem Cells *25*, 1136–1144.

Sirish, P., López, J.E., Li, N., Wong, A., Timofeyev, V., Young, J.N., Majdi, M., Li, R.A., Chen, H.S., and Chiamvimonvat, N. (2012). MicroRNA profiling predicts a variance in the proliferative potential of cardiac progenitor cells derived from neonatal and adult murine hearts. J. Mol. Cell. Cardiol. *52*, 264–272.

Stevens, K.R., Kreutziger, K.L., Dupras, S.K., Korte, F.S., Regnier, M., Muskheli, V., Nourse, M.B., Bendixen, K., Reinecke, H., and Murry, C.E. (2009). Physiological function and transplantation of scaffold-free and vascularized human cardiac muscle tissue. Proc. Natl. Acad. Sci. USA *106*, 16568–16573.

Sun, Y., Duffy, R., Lee, A., and Feinberg, A.W. (2013). Optimizing the structure and contractility of engineered skeletal muscle thin films. Acta Biomater. *9*, 7885–7894.

Thomas, S.P., Bircher-Lehmann, L., Thomas, S.A., Zhuang, J., Saffitz, J.E., and Kléber, A.G. (2000). Synthetic strands of neonatal mouse cardiac myocytes: structural and electrophysiological properties. Circ. Res. *87*, 467–473.

Tulloch, N.L., Muskheli, V., Razumova, M.V., Korte, F.S., Regnier, M., Hauch, K.D., Pabon, L., Reinecke, H., and Murry, C.E. (2011). Growth of engineered human myocardium with mechanical loading and vascular coculture. Circ. Res. *109*, 47–59.

Xi, J., Khalil, M., Shishechian, N., Hannes, T., Pfannkuche, K., Liang, H., Fatima, A., Haustein, M., Suhr, F., Bloch, W., et al. (2010). Comparison of contractile behavior of native murine ventricular tissue and cardiomyocytes derived from embryonic or induced pluripotent stem cells. FASEB J. *24*, 2739–2751.

Zhang, J., Wilson, G.F., Soerens, A.G., Koonce, C.H., Yu, J., Palecek, S.P., Thomson, J.A., and Kamp, T.J. (2009). Functional cardiomyocytes derived from human induced pluripotent stem cells. Circ. Res. *104*, e30–e41.

Zhang, D., Shadrin, I.Y., Lam, J., Xian, H.-Q., Snodgrass, H.R., and Bursac, N. (2013). Tissue-engineered cardiac patch for advanced functional maturation of human ESC-derived cardiomyocytes. Biomaterials *34*, 5813–5820.

Zimmermann, W.H., Melnychenko, I., and Eschenhagen, T. (2004). Engineered heart tissue for regeneration of diseased hearts. Biomaterials *25*, 1639–1647.